Journal of Fluids and Structures 52 (2015) 65–80

Contents lists available at ScienceDirect

Journal of Fluids and Structures

journal homepage: www.elsevier.com/locate/jfs

"Blind Test 3" calculations of the performance and wake development behind two in-line and offset model wind turbines

Per-Åge Krogstad [a,*], Lars Sætran [a], Muyiwa Samuel Adaramola [b]

[a] Department of Energy and Process Engineering, Norwegian University of Science and Technology NTNU, Trondheim, Norway
[b] Department of Ecology and Natural Resource Management, Norwegian University of Life Sciences, Ås, Norway

ARTICLE INFO

Article history:
Received 14 March 2014
Accepted 2 October 2014
Available online 15 November 2014

Keywords:
Wind turbines
Prediction method comparison
Blind test

ABSTRACT

This is a report on the comparison between measurement data and predictions presented at the "Blind Test 3" Workshop organized jointly by Nowitech and Norcowe in Bergen, 10 and 11 December, 2013. A number of researchers were invited to predict the performances and the wake development behind two model wind turbines that have been extensively tested at the Department of Energy and Process Engineering, NTNU. The turbines were arranged in-line, but slightly offset so that the wake of the upstream turbine only interacted with roughly half the area swept by the second rotor. This is a common event in most wind parks and produces flow fields that are both complicated and harmful for the downstream turbine. As expected it turned out to be a difficult flow to predict.

Contributions were received from five different groups using a range of methods, from fully resolved Reynolds averaged Computational Fluid Dynamics (CFD) models to Large Eddy Simulations (LES). The range of results was large but the overall trend is that the current methods predict the power generation as well as the thrust force reasonably well. But there is a large uncertainty in the prediction of the turbulence field in the wake. Hence, the LES method consistently performed better than the others.

1. Background

The aerodynamics tools available for engineers who design wind turbines and plan wind farms have matured significantly over the last two decades. However, their validity and range of trustworthy applications has not been well established. To help sort this out, reliable databases for comparison are needed. Full scale measurements are difficult to use for verifications since it is difficult to control all the boundary conditions needed in the simulations.

Most model tests in wind tunnels are performed at rather small scales, but a limited number of single turbine tests at intermediate scales are becoming available. The wind tunnel tests of the NREL two-bladed phase VI 10 m diameter turbine, completed in 2000, and the following blind comparison predictions by a large number of calculation methods (Simms et al., 2001) demonstrated how important it is to have detailed data to validate predictions against. The comparison showed that there was large uncertainty in the prediction methods, which called for more refined computer codes. Discussions of some of the issues that surfaced after the tests were presented in the special issue of *Wind Energy*, which was published in 2002

* Corresponding author.
E-mail address: per.a.krogstad@ntnu.no (P.-Å. Krogstad).

http://dx.doi.org/10.1016/j.jfluidstructs.2014.10.002
0889-9746/

(Schreck, 2002). The three-bladed 4.5 m MEXICO turbine (Snel et al., 2007; Schepers et al., 2010) is another example for which large amounts of useful data are available.

For wind farm planning, the wake development and wake-turbine interaction is the main concern and very little data on these problems is available at reasonable scale. As part of the joint Norwegian research programs denoted Nowitech and Norcowe it was decided to set up a model experiment to be used as a data source when testing out turbulence models or developing new prediction tools. Together, Nowitech and Norcowe are involved in research on most aspects of offshore wind turbine technology and have about 35 PhD or PostDoc members, many involved with wind turbine aerodynamics. Before the data was released it was deemed a good idea to arrange open blind comparison tests to find how the current prediction models used would perform if only the turbine geometry was known.

The main concerns when operating models of a large scale structure like a wind turbine in a wind tunnel are wall interference and Reynolds number effects. A rule of thumb is that a model front area should not exceed 10% of the tunnel cross section area for the measured drag forces not to be seriously affected by wall interference. This requirement was slightly violated for the test model, as the tower and swept rotor area for a single turbine is about 12% of the test section area. However, as a test case this was not considered very important since a faithful simulation would have to take the walls into account. Just as important as the area is the distance from the model to the walls. Therefore, the tower height to rotor diameter was chosen to be about correct for a full scale turbine. Hence interference effects from the ground would be about as expected at full scale.

With a nacelle centred roughly 80 cm above the floor, this leaves 1 m, or close to 1D between the rotor axis and the tunnel roof. Similarly, the distances to the nearest walls are about 1.4 m, corresponding to about 1.5D. As the flow develops downstream the wake may therefore be somewhat affected by the walls, which should to be accounted for in the predictions by imposing rigid side walls in the calculations.

The next concern is the large difference in Re that will affect the shear flows. To make the difference as small as possible, the model should be tested at as high velocity as possible and the relevant length scales should be as large as possible. Although the wind tunnel used is capable of operating at speeds up to about 30 m/s, the experience is that when operating at high speeds for extensive periods of time, the temperature rise in the flow will be so high that the air density and viscosity is affected. Therefore the model was designed to be operated at 10 m/s, which is a typical velocity for a full scale turbine. The model was designed to operate at a tip speed ratio of TSR=6, which is typical for a full scale turbine. In order to test the Reynolds number dependence of the flow, the performance of the turbine was measured over a wide tip speed range of reference velocities, from about U_{ref}=7 to 15 m/s. The power and thrust coefficients were found to be independent of Reynolds numbers for $U_{ref} > 9$ m/s (see e.g. Krogstad and Adaramola, 2012).

1.1. The blade geometry

To make the blade specification simple, the same airfoil was used all along the span. The airfoil selected is the 14% thick NREL S826 airfoil. It is originally intended to be used near the tip of a full scale turbine. The blades were made of aluminum and the maximum load on each blade was estimated to be about 15 N. It was assumed that the blades had sufficient stiffness so that geometrical changes due to the loads could be neglected. Therefore this slender airfoil could be used also for the root sections. The airfoil is shown in Fig. 1.

At the nacelle the blade has the usual circular cylinder used to fix the blade to the hub and allow pitch adjustments to be made. We expect that many prediction methods may have problems with reliable estimates of the flow where the geometry changes rapidly. Therefore no attempts were made in making a smooth transition from the circular section to the airfoil. Between the last circular section and the first NREL profile a simple linear transition region was added, producing a sharp corner at the base of the blade (see Fig. 2). It is expected that if this part is not properly resolved, the spanwise flow due to rotational effects will not be correctly captured, which might lead to severe problems when the blade operation approaches stall. Similarly, the tip of the blade was cut off sharply which will cause a challenge if the tip effects are not well handled.

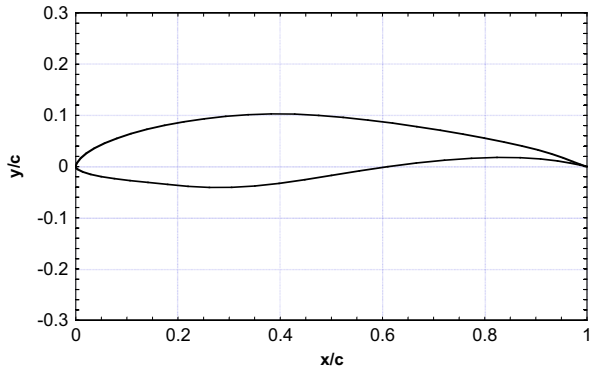

Fig. 1. Shape of the NREL S826 airfoil.

Fig. 2. Downstream turbine, facing downwind.

The model performance and wake data have been previously reported in Krogstad and Adaramola (2012), Adaramola and Krogstad (2011), Krogstad et al. (2010) and Krogstad and Lund (2012).

The blind tests started in 2011, when the geometry of a single turbine operating in a low turbulence, uniform flow was released. The wind turbine models used for these tests were designed in 2008 with the specific aim to form a test case for prediction methods. In particular it was considered important to produce good experimental data to act as a database that allows the ability of various turbulence models aimed at predicting the turbine wake to be verified. Therefore this is not a typical wind turbine layout, since measurement and wind tunnel restrictions, combined with test case challenges, had to be considered. For a test case it was important to use a simple geometry for maximum numerical accuracy in the description of the turbine, while at the same time introducing effects that might be difficult to handle by a prediction method. This led to the design shown in Fig. 2. As may be seen from the photo, the turbine has 3 blades and the rotor sits on top of a stepped tower consisting of 4 cylinders of different diameters. The nacelle is also circular with a diameter of $d=90$ mm. It has an almost semi-spherical hub cover at the front and back. The rotor diameter is $D=0.894$ m and the centre of the rotor is located $z=0.817$ m above the floor level.

For the first blind test, BT1, reported in Krogstad and Eriksen (2013), the participants were asked to predict the turbine performance characteristics as well as the wake development down to five diameters downstream of the rotor plane.

BT1 turned out to be very popular with the participants and second, more complicated test was called for. For the second blind test, BT2, held in 2012 (results presented in Pierella et al., 2014) a second turbine was designed with the same blades, but with a modified nacelle and tower design. The main reason for the changed geometry was that the turbines were driven from a motor/generator located under the tunnel floor by means of a belt. For the first turbine the belt was running freely behind the tower. With the new tower design the belt could be accommodated inside the tower, thereby causing less disturbance to the flow in the wake. The second turbine is shown in Fig. 3. Because it has a somewhat wider nacelle, but uses the same blades, this turbine has a slightly larger rotor diameter of $D=0.944$ m. To some extent this changed the performance envelope of the turbine, mainly by making the stall characteristics more dramatic. The model rotor centre height is the same as for the other turbine.

The models were mounted in-line, with a separation of only 3 diameters and tested in the wind tunnel that has a test section which is almost 12 m long. The height is about 2 m and the width almost 3 m. The short distance between the turbines was necessary to allow a reasonable fetch for the wake to develop downstream of the second turbine. For full details on the wind tunnel and instrumentation, see one of the references, Krogstad and Adaramola (2012) or Adaramola and Krogstad (2011).

1.2. Test case description

The turbine with the thick tower was placed upstream, two diameters from the entrance to the tunnel test section. We will denote this turbine T_1 and this turbine has a rotor diameter of $D_1=0.944$ m. When seen from upstream, this turbine was located $\Delta y=0.20$ m off the centre line towards the left.

Sketches of the layout are given in Figs. 4 and 5. Fig. 6 shows a picture of the turbines mounted in the tunnel.

The turbine with the stepped tower, denoted turbine T_2, with $D_2=0.894$ m, was placed three diameters further downstream and shifted $\Delta y=0.20$ m off the centre line towards the right from the centre line. This gives a total offset between the turbines of $\Delta y=0.40$ m, and so the projected area of the upstream rotor covers exactly 50% of the downstream rotor area. Both turbines were rotating in the clockwise direction when seen from behind. With the two turbines in the tunnel it may be argued that the blockage effect has increased. However, since they are located at different streamwise positions, the total blockage will not be as high as the one computed by using the total area seen when looking down the test section (which is about 17%). Since the wake flow from the first turbine is allowed to recover and re-energize somewhat

Fig. 3. Upstream turbine, looking into the wind.

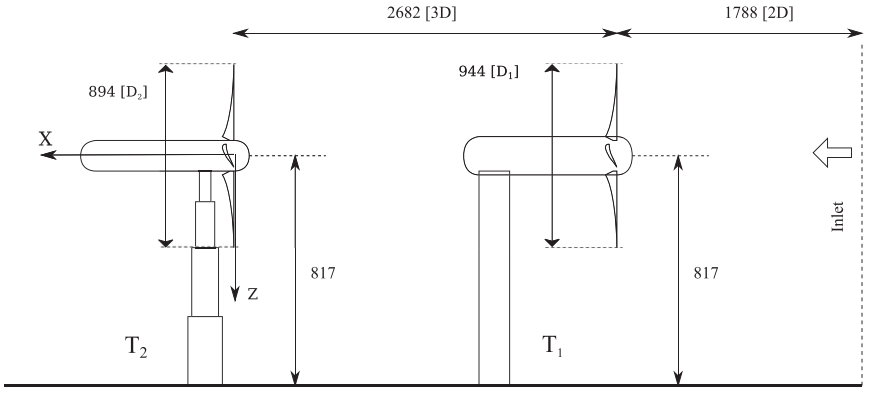

Fig. 4. Wind tunnel placement of the turbines seen from the side.

due to the significant distance between the turbines and due to the spanwise offset which generates a highly asymmetric wake behind the second turbine, the effective blockage ratio may be somewhere between the value for a single turbine (12%) and the visual blockage for the two (17%). In any case, the only way to incorporate the blockage effects on the flow is by faithfully reproducing the entire flow geometry.

The coordinate system used is shown in Figs. 4 and 5. The origin is placed in the plane swept by the T_2 rotor, with x pointing in the streamwise direction. The vertical origin is at the height of the rotor centres and the spanwise origin is at the tunnel centre line. For normalization of the streamwise coordinate (x), e.g. the distance between the two turbines and positions for the measurement stations, we have used the diameter of the second turbine, $D = D_2 = 0.894$ m. For reference velocity, the development of the velocity along the rotor axis upstream of the first turbine was measured. Using $U(x) = U_{ref}(1-a)$ and extrapolating this distribution upstream to where the axial induction factor, a, reached zero, U_{ref} was found.

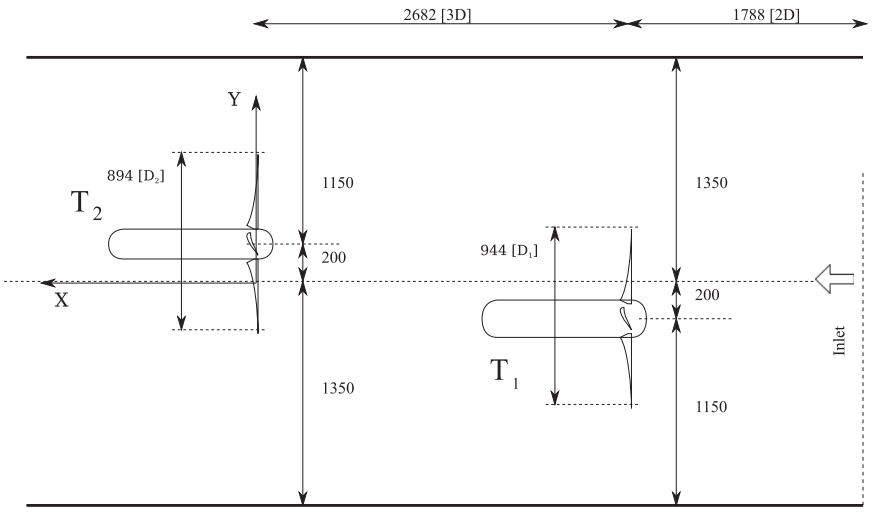

Fig. 5. Wind tunnel test section layout seen from the above.

Fig. 6. Model in the wind tunnel.

The empty wind tunnel has a low turbulence level of 0.23% which is almost constant along the test section. In order to make the conditions more similar to the atmospheric conditions where wind turbines are operating, background turbulence was generated using a large scale bi-planar mesh. The mesh size was $M=0.24$ m and the solidity was 35%. The grid was mounted at the entrance to the test section and may be seen in Fig. 3. This gave a streamwise turbulence level at the location of T_1 of $T_u = 100\%\sqrt{\langle u^2\rangle}/\langle U\rangle = 10\%$. (Here u is the fluctuating and $\langle U\rangle$ the mean streamwise velocities. $\langle\cdot\rangle$ indicates time averaging.) Since there is no mechanism to maintain the turbulence energy in the streamwise direction, the turbulence level depends on the position and so the level had dropped to about 5% at the location of the second turbine. The grid flow is documented in Davidson and Krogstad (2008).

A web site was made available to the participants which contains a test case description, tables describing the geometries and CAD files for the blades and nacelles. Except for the geometry specifications and wind tunnel inlet conditions, no further information was given by the organizers. Thus, if the participants needed e.g. lookup tables to determine the load distributions on the blades, they would have to generate this information themselves. The way this was obtained would have impact on the results. Hence, the first compulsory output was predictions of the power and thrust coefficients.

The main focus of the blind test was, however, on the wake development behind the downstream turbine. The flow behind T_1 had been the main task for the first test, so the accuracy of the predicted inflow to T_2 was roughly known (see Krogstad and Eriksen, 2013). The participants were asked to provide profiles of the mean velocity, U/U_{ref}, and turbulent kinetic energy, $k^2/U_{ref}^2 = \frac{1}{2}\left(u_x^2+u_y^2+u_z^2\right)/U_{ref}^2$, or preferably all the normalized stresses u_i^2/U_{ref}^2, at two downstream positions, $x/D=1$ and 3, measured from the rotor plane of T_2. The data should be provided along a horizontal line through the centre of the wake when T_1 was operating at TSR=6 (peak performance) and TSR=3.5, 4.75 and 8 for T_2.

The rotor thrust predictions were compared with forces measured by a 6 component balance on which the model was mounted. The drag of the tower and nacelle was subtracted from the measurements according to separate measurements performed on the turbine when the blades had been removed. The power coefficient was measured using a torque transducer mounted directly onto the rotor shaft which also provided pulses to measure the speed of rotation. Velocities were measured using x-wire anemometry after the signals had been suitably amplified and filtered. The data was sampled for 60 s at 14 kHz, giving a total of 840 000 samples per measurement point. For verification, some of the measurements were repeated using pitot-static tubes and laser Doppler anemometry. The uncertainty in the measurements of the mean velocity was estimated to be less than $\pm 4.6\%$ of U_{ref} and $\pm 5.9\%$ of U_{ref}^2 for k^2. These values were estimated for the low turbulence case at $X/D = 1$ at the position where the mean velocity had its maximum velocity defect and the kinetic energy had its peak value. The error estimates include uncertainties in calibration data as well as the statistical uncertainty computed according to the methods of Benedict and Gould (1996).

For the power coefficient measurements, C_P, the uncertainty was found to be less than $\pm 4\%$ when T_1 was operated in the range $1 < \mathrm{TSR} < 10$ and for T_2 over the range $2 < \mathrm{TSR} < 7$. The uncertainty in the measurements of the thrust coefficient, C_T, was found to be almost constant over the measurement ranges and was estimated to be within $\pm 2\%$.

In the empty wind tunnel the incoming free stream velocity was measured to be uniform to within $\pm 1\%$ over the area swept by the rotor and the turbulence intensity in the empty wind tunnel was $\sqrt{\langle u^2 \rangle}/U_{ref} = 0.23\%$ at the position of the rotor of T_1, decreasing to 0.22% where T_2 was placed. With the grid installed, the turbulence field was measured from the grid to the exit of the test section. The turbulence intensity, integral length scales and dissipation rates in the empty tunnel at the T_1 position only were given, making the calculation of turbulence decay in a uniform flow part of the problem.

2. Participants and methods

Calculations were submitted by five groups. In order to start the wake calculations, the power and thrust coefficients of the turbines must first be estimated. This was therefore compulsory output. Two participants resolved the flow down to the boundary layer on the turbine blades, while the rest relied to some extent on a Blade Element Momentum method calculation.

For the methods that use some imbedded force method, estimates of the airfoil performance were needed, e.g. using software such as XFOIL (http://web.mit.edu/drela/Public/web/xfoil/). However, suggested values of airfoil lift and drag coefficients from unpublished experimental data were also provided.

Below is a short list of the participants and the essences of their methods.

2.1. Acona flow technology

E. Manger of Acona Flow Technology, Skien, Norway, modelled the entire experimental setup, including the towers and nacelles with the turbines located inside the test section. The rotors were included in a short cylindrical sliding mesh within a fixed grid. The boundary layers on the blades were resolved down to $y^+ \approx 5$. The wind tunnel domain was meshed using hexcore mesh extending all the way to the wall, while polyhedral mesh was used for the two rotating domains. The flow was solved with an incompressible model using the *Ansys Fluent v*.14-5 software. The k–ω SST turbulence model with standard coefficients was used to model the turbulent field. The final mesh used approximately 12 million cells. The computations were rather time consuming and therefore only Case A was completed in time for the meeting. The method is described in more detail in Manger (2011).

2.2. DTU mechanical engineering

The group of collaborators from DTU, Lyngby, Denmark, and KTH, Stockholm, Sweden, delivered data for a combined actuator line/Large Eddy Simulation (LES) using a program called *EllipSys3D*. (These predictions will be denoted DTU.) This program uses a block structured finite volume approach. The time increment was sufficiently small so that the tip of the blade advanced less than half a cell per step. The blades are represented by forces along rotating lines and the loads were estimated from their own unpublished measurements for the NREL S826 airfoil. In addition a force line was added to account for the drag and lift forces of the tower.

The computational domain is a regular Cartesian grid divided into 750 blocks using a total of 24.5 million mesh points. The tunnel walls are included in the calculations, but the nacelles are missing. The tunnel turbulence was simulated by inserting synthetic turbulence 1.5 diameters upstream of the first turbine and the level was adjusted to match the experimental conditions at the T_1 rotor plane. Four grid resolutions were tested to find the required density for grid independency. Further documentation of the method used may be found in Troldborg et al. (2010).

2.3. GexCon

M. Khalil of GexCon, Bergen, Norway, performed calculations using the software package *FLACS-Wind* which is developed by GexCon. This is an incompressible transient CFD solver which in this case used the standard k–ϵ turbulence model with standard coefficients. The computational domain was similar to the wind tunnel dimensions, but the increase in tunnel

height to compensate for the growth of side wall boundary layers was not included. The rotor was represented as an actuator disk and the disk data was obtained using a BEM method. The effects of the towers and nacelles were not included in the simulations. A total of 0.8 million cells in a structured grid were used for the calculations. See Khalil and Sælen (2013) for more details about the method used.

2.4. CD-adapco

S. Evans from CD-adapco, London, UK, provided incompressible predictions using their own software Star-CCM+. Around the rotors, cylindrical domains were created so that the arbitrary sliding interface functionality of STAR-CCM+ could be used to model the rotor motion. A polyhedral mesh was created containing 14 million mesh elements with the boundary layer on the blades being resolved down to a Y^+ value of less than 2, dependent on the operating conditions. Predictions were provided using the k–ω SST Detached Eddy Simulation (DES) model with curvature corrections. The mesh was created in such a way that the DES model operated in LES mode in the wake regions of the flow. The simulation ran in a two-step approach. Firstly, the case was run using a steady approach with multiple rotating frames. After the simulation was considered to be sufficiently initialized, it was switched to transient simulation. For a description of how the software is used for rotating flows, see Mendonca et al. (2012).

2.5. CMR

A. Hallanger and I.Ø. Sand of CMR Instrumentation, Bergen, Norway, used an incompressible CFD code called Music which has been developed in-house. The rotors, including the hubs, were modelled in the wind tunnel confinement, but the rest of the nacelle, as well as the towers, were omitted. The forces on the blades were estimated using a generalized Blade Element Momentum model with rotation and included as source terms in the axial and rotational momentum conservation equations. A total of 30 elements were distributed along the radial direction of the blade and a total of 0.5 million structured grid nodes were used to represent the wind tunnel test section with the turbine rotors. The turbulence was described using the standard k–ϵ model with a sub-grid model. The standard Launder–Spalding constants were applied. The turbulence intensity and length scales for the two test cases were applied as specified in the case description. The calculations were performed in a steady state mode and the final data was derived by averaging predictions obtained at every 15° for a full 360° set of data. The method and its details are described in Hallanger and Sand (2013).

3. Results

3.1. Predicted turbine performances

We start by presenting the results for the turbine performances for Case A, i.e. with the low background turbulence level. The power coefficients $C_{P_i} = 8P_i/(\pi\rho U_{ref}^3 D_i^2)$ are shown in Fig. 7(a) and the thrust coefficients $C_{T_i} = 8F_i/(\pi\rho U_{ref}^2 D_i^2)$ in Fig. 7(b). (Here P_i is the power generated by turbine T_i as measured directly on the rotor axis at the nacelle. F_i is the thrust force on the rotor obtained by measuring the total drag force of the turbine and subtracting the drag generated by the nacelle and tower. U_{ref} is the reference velocity seen by T_1 and this velocity is used as velocity scale for both turbines. D_i is the rotor diameter of turbine T_i.)

The symbols used will always have the same colour and shapes in all figures, with filled symbols for the upstream turbine and open symbols for T_2. The measurements will always be presented as black circles. Finally we mention that for the measurements of C_{P_2} and C_{T_2}, the operating conditions for T_1 were kept constant at a tip speed ratio of TSR$=\omega D_1/(2U_{ref})=6$. The speed of rotation for T_2 was then varied in order to cover the required TSR range.

Even though the two turbines have the same blades, the shape of the C_P curves is seen to be different. The upstream turbine shows a rapid drop when TSR falls below 4. This is due to the sudden onset of stall (see Krogstad and Lund, 2012). For T_2, this development appears to be less dramatic. One may therefore speculate that this is due to a much higher turbulence level felt in the incoming flow to T_2 which has generated a more gradual separation development. However, when tested alone in Blind test 1, it was seen that turbine T_2 has a much smoother C_P curve than the one shown for T_1 (see Krogstad and Eriksen, 2013). The only difference in the two rotors is that T_1 has a slightly larger diameter and thus the blade design is not optimal for T_1. The effects will, however, be included in the predictions, since the geometry of all components were specified in the invitation.

The spread in the power predictions for the upstream turbine is about the same as in the two previous blind tests. This is surprisingly large, considering that most of the participants have already preformed predictions for these turbines before and know the performance curves. The data for the second turbine predictions vary by more than 50% in some regions, but this is more understandable, since we here have the most complicated test case so far. However, some of the predictions for T_2 are in fact very good at high tip speeds, e.g. the curves obtained by DTU, CMR Instrumentation and CD-adapco for TSR >6.

For the very low TSRs, where the flow over the blades is severely stalled, the deviation from the measurements is mostly small. It was expected that one of the principal problems would be to predict the onset of stall, for reasons mentioned earlier. In a previous study (Krogstad and Lund, 2012), the first signs of stall when the T_2 turbine operates alone were found to occur around TSR$=4$ and this is where the largest uncertainties in the predictions are found. But for the deep stall region for TSR <3, all methods behave well. This suggests that the airfoil data used in most predictions are reasonably correct in

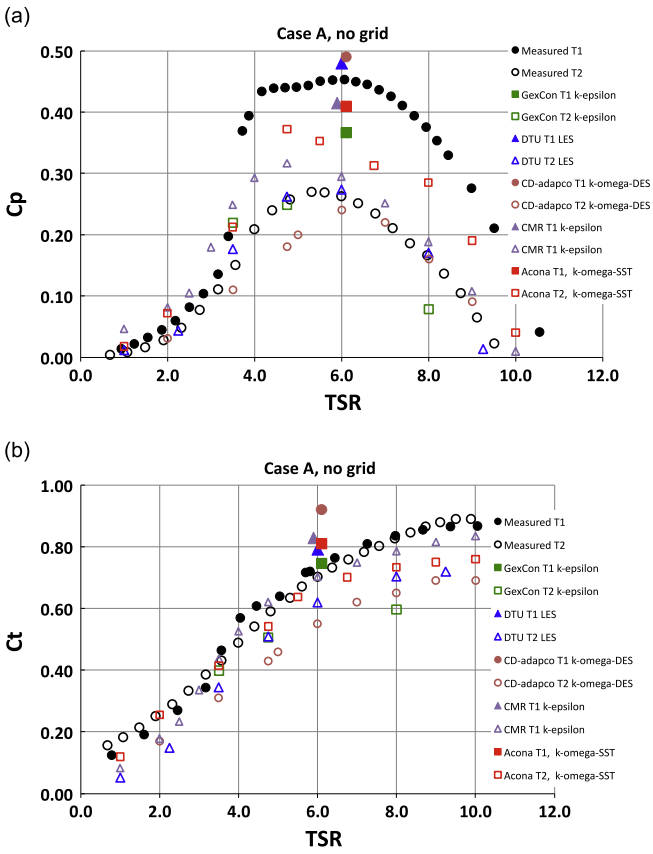

Fig. 7. Turbine performances, Case A, low turbulence level. (a) Power coefficient, $C_{P_i} = 8P_i/\left(\pi\rho U_{ref}^3 D_i^2\right)$, (b) thrust coefficient, $C_{T_i} = 8F_i/\left(\pi\rho U_{ref}^2 D_i^2\right)$. P_i is the power generated by turbine T_i and F_i is the thrust force on the rotor. U_{ref} is the reference velocity seen by T_1. D_i is the rotor diameter of turbine T_i.

the low and very high angle of attack regions. However, predictions of the stall development may have been quite different in the methods used. Unfortunately this information was not requested from the participants.

The fully resolved predictions of Acona and CD-adapco do not agree. Acona predicts consistently the highest C_P while the predictions by CD-adapco are generally low. Since they both used the k–ω SST turbulence model in the blade boundary layers, this points to significant differences in the numerical grids constructed.

Looking at the thrust coefficient (Fig. 7(b)), the measurements of the upstream turbine again show that something happens to the flow as TSR is reduced below 4. Except for a short region here, the C_T data for both turbines are very similar. This is puzzling, since the velocity fields seen by the two rotors are very different. Despite this, the coefficients are the same when scaled with the same parameters, showing that the physical forces are in fact almost identical even though the momentum available at T_2 ought to be less than for T_1.

The general trend is that C_T is mainly over-predicted for the T_1 turbine, but under-predicted for T_2. GexCon has matched the force on turbine T_1 very well, but underpredicts the forces on T_2 dramatically at TSR=8.

Next we present the performance data for the case with high turbulence level, Case B. The measurements indicate that the peak performance of the upstream turbine has been slightly reduced (Fig. 8(a)) and the shape is seen to be smoother, again suggesting that the free stream turbulence significantly affects the onset of stall on the blades. None of the performances predicted for T_1 appears to be sensitive to the freestream level. The same applies to the T_2 predictions.

However, the measured performance of T_2 is slightly increased by the turbulence. This is consistent with the reduction in energy extraction by T_1. The turbulence effect shows even more clearly in the measurements for C_T (Fig. 8(b)), which indicate a dramatic sensitivity to the freestream turbulence for both turbines. Compared to Case A, C_T for T_1 is reduced by between 10% and 15%, and thus C_T for T_2 has increased by about the same amount.

4. Wake data

4.1. Operation at peak performance, $TSR_1=6$, $TSR_2=4.75$

The participants were asked to predict the wake development behind turbine T_2 when T_1 was operating at its design TSR and T_2 was operating at TSR=3.5, 4.75, and 8.0. TSR=4.75 is close to the peak performance for T_2 and will be presented first.

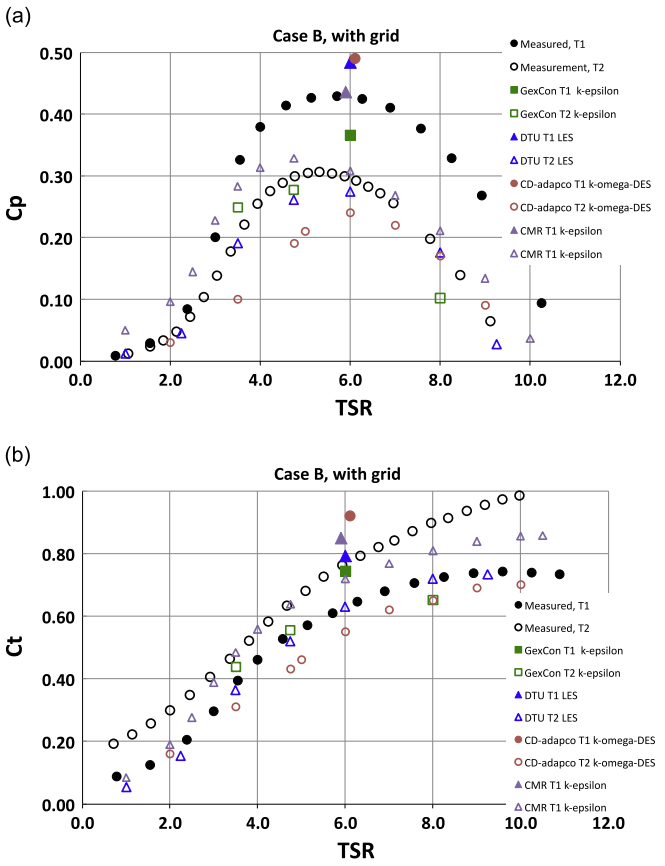

Fig. 8. Turbine performances, Case B, grid generated turbulence. (a) Power coefficient, $C_{P_i} = 8P_i/\left(\pi\rho U_{ref}^3 D_i^2\right)$, (b) thrust coefficient, $C_{T_i} = 8F_i/\left(\rho U_{ref}^2 D_i^2\right)$. P_i is the power generated by turbine T_i and F_i is the thrust force on the rotor. U_{ref} is the reference velocity seen by T_1. D_i is the rotor diameter of turbine T_i.

This should be the operating condition that generates the most homogeneous wake and therefore be the simplest case to predict. However, only part of the wake from T_1 hits the rotor of T_2, so T_2 will see a very inhomogeneous inflow and therefore the wake becomes quite complicated also in this case.

Output of mean velocities and kinetic energy were requested for both Cases A and B at $X/D=1$ and 3 downstream of T_2. (The diameter used to scale the distances in the wake is $D=0.894$ m of T_2.) Since for most measurements only two of the three normal stresses that form the turbulent kinetic energy, $k=(\langle u_x^2\rangle+\langle u_r^2\rangle+\langle u_\theta^2\rangle)/2$, were measured, we present only the streamwise normal component $\langle u_x^2\rangle$ here. For the predictions where the individual stresses were not part of the solution, we have used the isotropic normal stress approximation $\langle u_x^2\rangle \approx 2k/3$ to enable a comparison. The measurements where all three components were obtained have shown that this is a very good approximation in the wake, as shown in Fig. 9. The figure shows two sets of data for Case A at $X/D=1$. One traverse was done with the probe aligned to measure $\langle u_x^2\rangle$ and $\langle u_r^2\rangle$. The next was done with the probe rotated 90° to measure $\langle u_x^2\rangle$ and $\langle u_\theta^2\rangle$. From this k was computed (open black circles) and compared to the estimate $k=3\langle u_x^2\rangle/2$ (black dots). The two estimates collapse very well with only small differences at the far righthand side. (It should be kept in mind that the ordinate axis is logarithmic, so the numerical values here are very small.) The two data sets for $\langle u_x^2\rangle$ may also be compared (black and blue squares) to verify that the repeatability in the measurements is good.

The first station for which data was requested was at $X/D=1$ downstream of the rotor plane of T_1 (see Figs. 4 and 5 for coordinate system definition). The mean velocity profiles measured along a horizontal line parallel to the floor at the elevation of the hub axis are shown in Fig. 10(a) for Case A and Fig. 10(b) for Case B.

There are a few obvious observations that may be made immediately. Compared to the wake behind a single turbine operating at its best performance, this is a much more complicated wake. The centre of turbine T_1 is located at $y/R=-0.45$ and the rotor extends from $y/R=-1.50$ to $y/R=+0.61$. T_2 has its centre at $y/R=+0.45$ with a rotor that spans from $y/R=-0.55$ to $y/R=+1.45$. The outer edges of the combined wake are quite evident, but the central part is a mix of influences from the two wakes.

As expected, the wake for Case B is much smoother than for Case A. This smoothing effect comes out much clearer in the predictions than in the measurements if we compare e.g. the predictions by GexCon and CMR with the measurements (Fig. 10(b)). Acona did not provide predictions for Case B. The LES predictions by DTU appear to have captured all the details

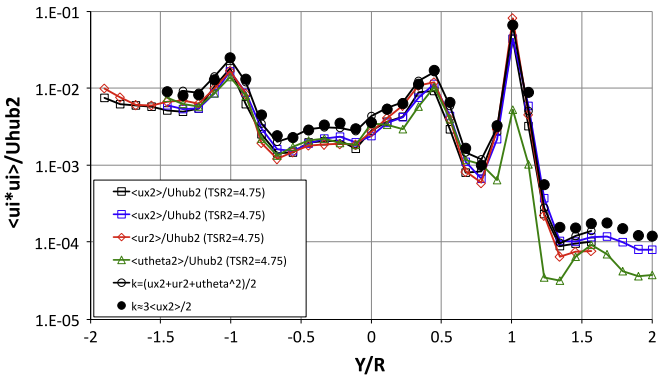

Fig. 9. Stresses and estimates of turbulent kinetic energy. (For interpretation of the references to colour in this figure caption, the reader is referred to the web version of this paper.)

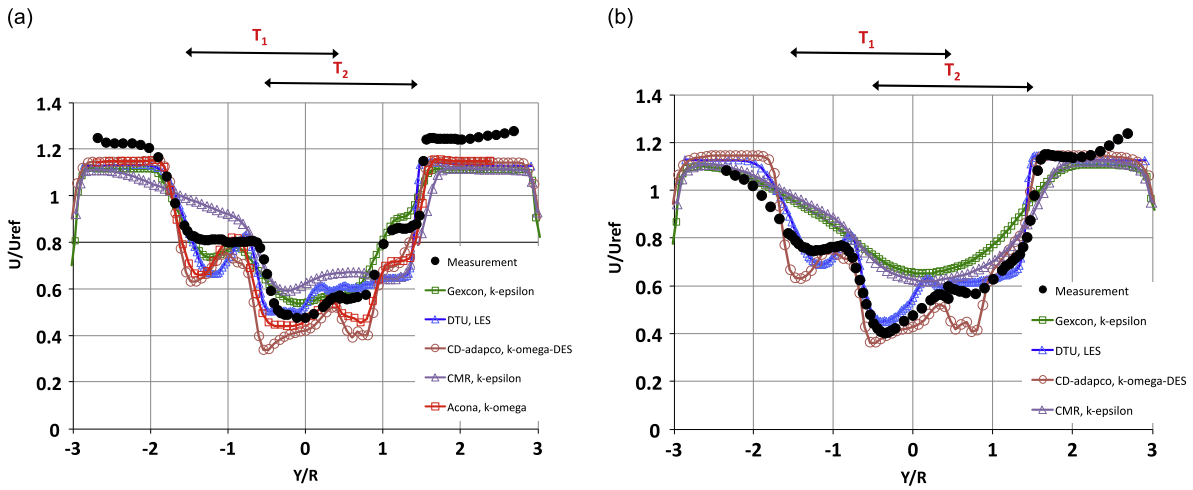

Fig. 10. Mean velocity profiles for $TSR_1=6$, $TSR_2=4.75$ at $X/D=1$. (a) Case A, (b) Case B. (For interpretation of the references to colour in this figure caption, the reader is referred to the web version of this paper.)

of the wakes very well for both cases and the accuracy of the CD-adapco DES predictions are almost as good. The GexCon method performs very well in Case A, avoiding the oscillations found in the predictions of Acona, CD-adapco and to some extent in the DTU results.

The differences in the mean velocity profiles are reflected in the turbulent stresses as well. These are shown in Fig. 11(a) for Case A and Fig. 11(b) for Case B. While the methods of Acona, CD-adapco and DTU appear to have captured most of the details of the stress distributions for both cases, the level of accuracy relative to the measurements in the GexCon and CMR predictions is not good. The energy level predicted by DTU is mostly close to the measurements, but computations by the Acon and CD-adapco methods are predominantly low.

Next we move downstream to $X/D=3$. The mean velocity profiles along a horizontal diagonal are shown in Fig. 12(a) for Case A and Fig. 12(b) for Case B. Diffusion has now significantly modified the flows and so the measured mean velocity profiles show very little detail in both cases. The effect of diffusion appears to be overestimated by the CMR method for both cases, while the predictions by Acona seem to have the opposite problem with a profile that are very similar to those at $X/D=1$. While the method by GexCon performs very well in Case A, diffusion is much too strong in Case B. However, the DES of CD-adapco produces profiles that are very close to the LES by DTU for both cases.

Fig. 13(a) shows the turbulent stresses for Case A and Fig. 13(b) for Case B. The figures show that the LES method of DTU and the DES of CD-adapco perform best when it comes to reproducing the sharp energy peaks, although the fine details near the centre in Case A are missing in both predictions. Again the results for Cases A and B are very different in the predictions by the GexCon method. But the predictions of CMR are now closer to the measurements for both cases compared to those at $X/D=1$ (Fig. 11(a) and (b)) although the details of the tip vortices are missing. Acona produced the correct stress distribution for Case A, but again the level is much too low.

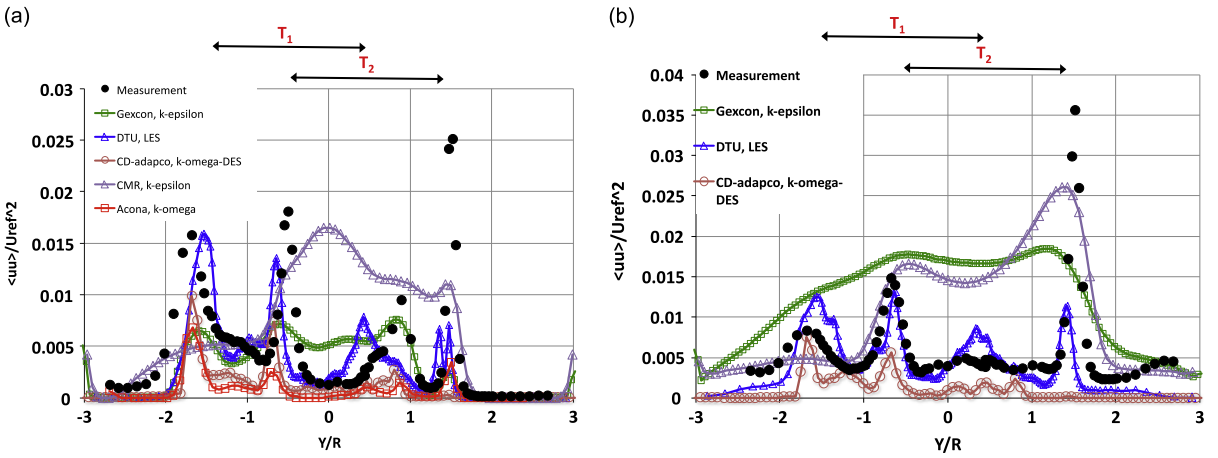

Fig. 11. Turbulent stress $\langle u_x^2 \rangle$ for $TSR_1 = 6$, $TSR_2 = 4.75$ at $X/D = 1$. (a) Case A, (b) Case B. (For interpretation of the references to colour in this figure caption, the reader is referred to the web version of this paper.)

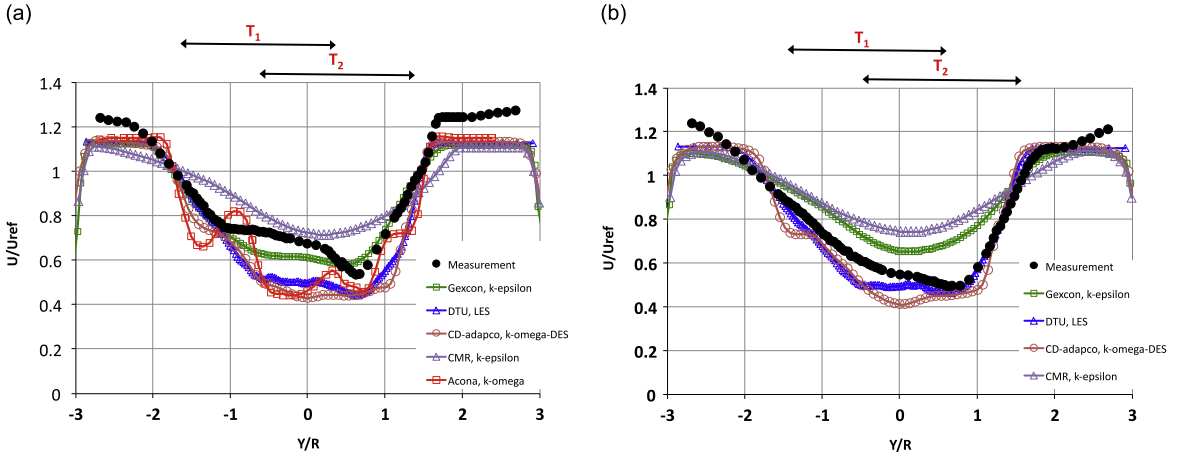

Fig. 12. Mean velocity profiles for $TSR_1 = 6$, $TSR_2 = 4.75$ at $X/D = 3$. (a) Case A, (b) Case B. (For interpretation of the references to colour in this figure caption, the reader is referred to the web version of this paper.)

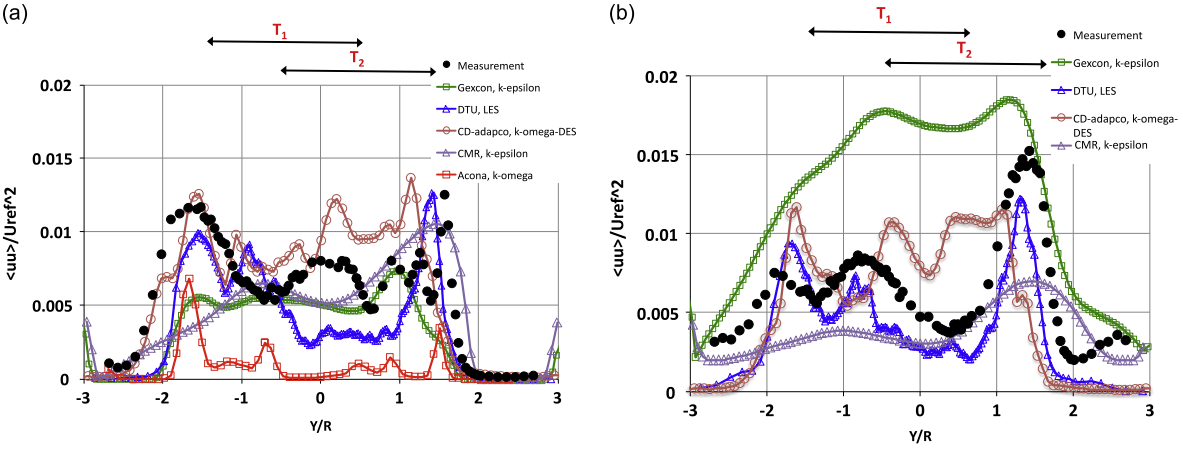

Fig. 13. Turbulent stress $\langle u_x^2 \rangle$ for $TSR_1 = 6$, $TSR_2 = 4.75$ at $X/D = 3$. (a) Case A, (b) Case B. (For interpretation of the references to colour in this figure caption, the reader is referred to the web version of this paper.)

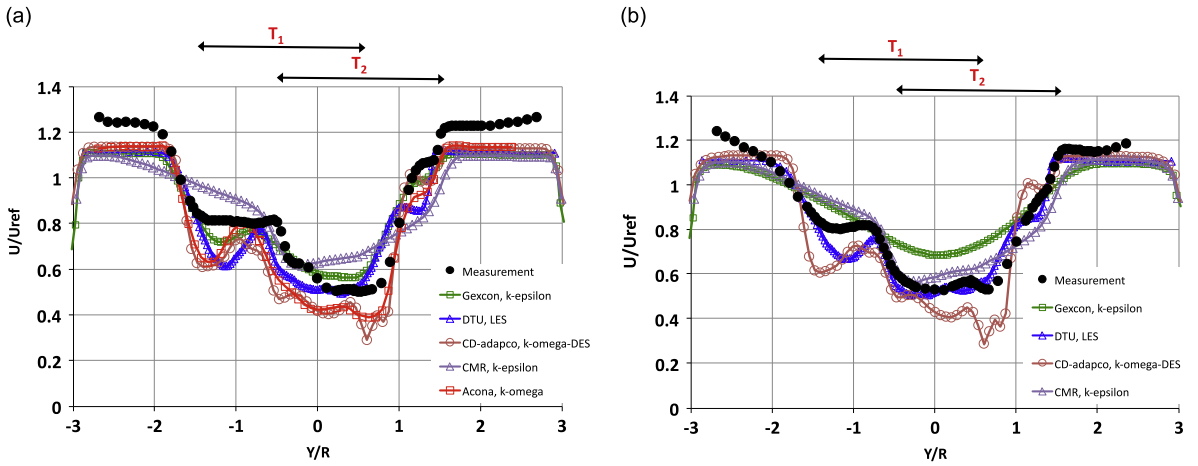

Fig. 14. Mean velocity profiles for $TSR_1=6$, $TSR_2=3.50$ at $X/D=1$. (a) Case A, (b) Case B. (For interpretation of the references to colour in this figure caption, the reader is referred to the web version of this paper.)

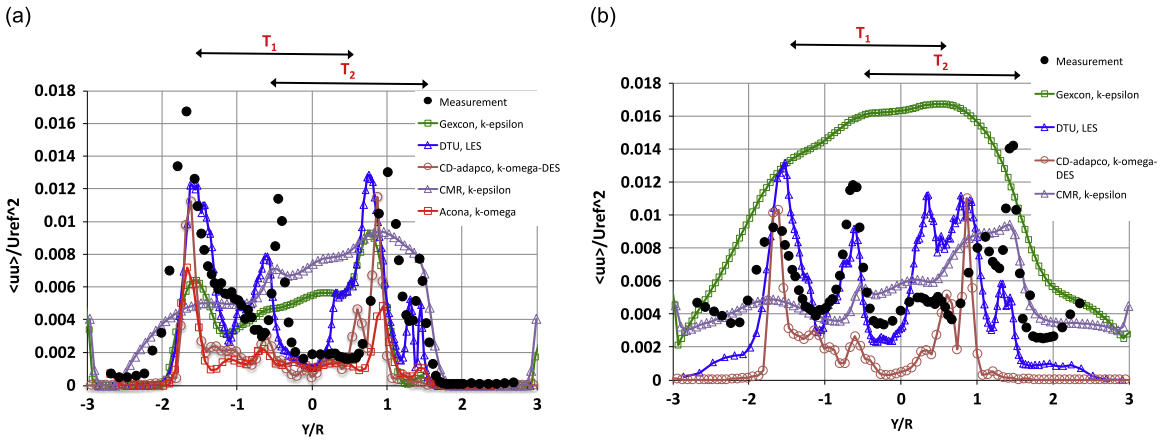

Fig. 15. Turbulent stress $\langle u_x^2 \rangle$ for $TSR_1=6$, $TSR_2=3.50$ at $X/D=1$. (a) Case A, (b) Case B. (For interpretation of the references to colour in this figure caption, the reader is referred to the web version of this paper.)

4.2. Profiles when T_2 is partly stalled; $TSR_1=6$, $TSR_2=3.50$

Next the results when turbine T_1 is operating at its best performance ($TSR_1=6$), but turbine 2 operates well into its stall regime ($TSR_2=3.50$) will be presented. This case was included because it was judged to be the most complicated case to predict. T_2 is stalling, but is not fully stalled, so the power production is reduced roughly by a factor two compared to the previous case.

We start by inspecting the profiles at $X/D=1$ (see Fig. 14(a) for Case A and Fig. 14(b) for Case B). Surprisingly it was found that the mean velocity profiles are very similar to the ones observed when TSR_2 was 4.75 (see Fig. 10(a) and (b)). The shape has been captured quite well by all methods for Case A, although slightly less successful by the CMR model. In the turbulent case (Case B) the LES of DTU reproduces the profile very well except for a small region near $y/R \approx -1$.

The stress profiles do not appear to be very sensitive to the changes in TSR either. The method of GexCon has captured the energy from the tip vortices at the outer edges of the combined wake in Case A, but has lost all characteristic details in Case B. DTU on the other hand has produced a high level of energy in the region $0 < y/R < 1$ for Case B, which does not appear in the measurements and only suggest a weak vortex at the outer right hand boundary. The Acona, CD-adapco and DTU methods all predict the major peaks, although the positions and levels are not always correct (Fig. 15).

Next we briefly show the results at $X/D=3$ for the same operating conditions (Figs. 16(a) to 17(b)). It is obvious that turbulent diffusion between $X/D=1$ and 3 has smoothed out most of the fine details both in the mean velocity and the stress profiles. The CD-adapco predictions produce mean velocity profiles that are virtually identical to those by DTU. For Case B the GexCon model responds too strongly to the increased background turbulence level with too much diffusion and too strong turbulence production. However, the method performs quite well for Case A.

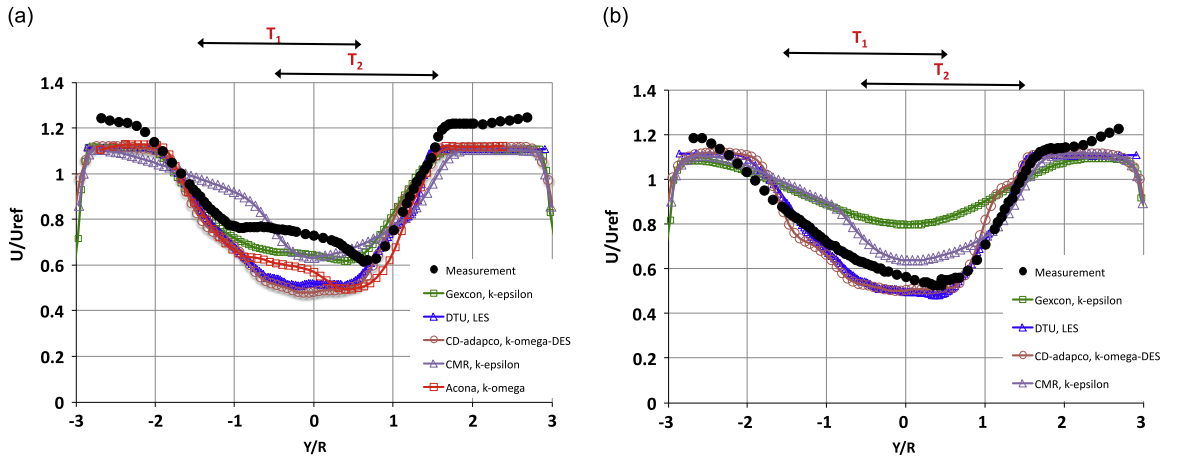

Fig. 16. Mean velocity profiles for $TSR_1=6$, $TSR_2=3.50$ at $X/D=3$. (a) Case A, (b) Case B. (For interpretation of the references to colour in this figure caption, the reader is referred to the web version of this paper.)

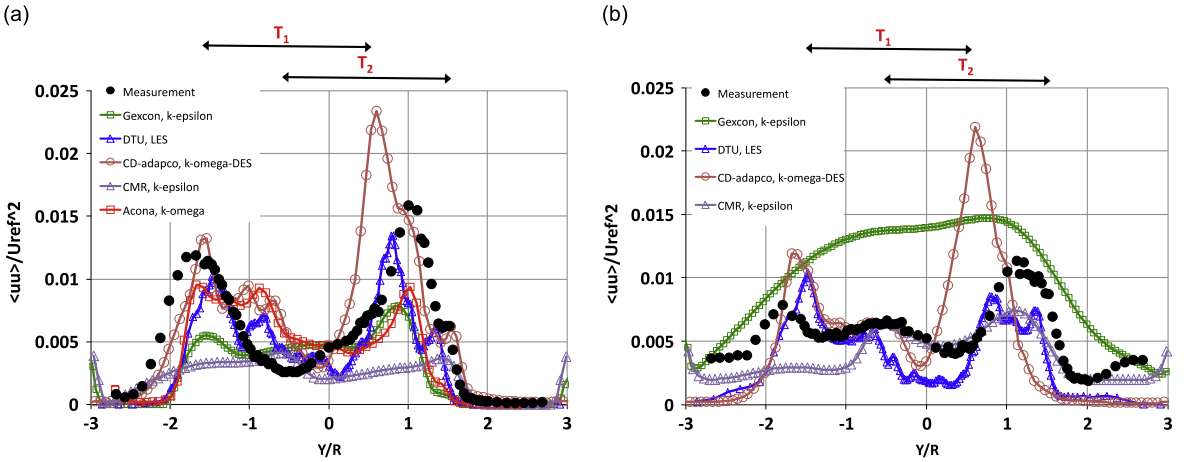

Fig. 17. Turbulent stress $\langle u_x^2 \rangle$ for $TSR_1=6$, $TSR_2=3.50$ at $X/D=3$. (a) Case A, (b) Case B. (For interpretation of the references to colour in this figure caption, the reader is referred to the web version of this paper.)

4.3. *Profiles where T_2 operates partly as a propeller; $TSR_1=6$, $TSR_2=8.00$*

The final test case was when turbine T_2 operates at a high speed of rotation. In this case the energy produced by T_2 is about the same as when it operated at TSR=3.5. But now the inner part of the rotor starts to feed energy into the flow by operating as a propeller, while the outer sections of the blades work hard to extract energy from the flow. Even though the local angle of attack is low in the tip region, the very high relative velocity causes high loads on the blades and this produces high C_T values. Hence we expect a very different set of profiles where the velocity defect is very small in the centre and quite strong near the tips of the T_2 blades.

The mean velocity profiles at $X/D=1$ are shown in Fig. 18(a) for Case A and Fig. 18(b) for Case B. It is immediately observed that these profiles show a distinct waviness in the right hand part, due to the mixed operating mode of turbine T_2. It is also apparent that this flow is considerably less affected by the free stream turbulence than the other flows. These details are captured by most methods, and this time the mean velocity profiles generated by the CD-adapco and DTU LES methods are also almost identical for the two flows. The prediction of the maximum velocity defect from the left hand side of the wake behind T_2, found at $Y/D\approx -0.5$, is however much too strong in most predictions. The predictions by CD-adapco reproduce the wake behind T_2 very well for both cases. The predictions by the GexCon and CMR methods, which both use the k–ϵ turbulence model, produce much smoother profiles than the other models and show lower accuracy for Case B.

The stress profiles (Fig. 19(a) and (b)) reflect the complexity of the mean flow as it has a number of very high peaks. The locations are captured well by the CD-adapco and DTU predictions for both cases. While DTU over-predicts the peak at $y/R\approx -0.5$ by roughly a factor two, CD-adapco predicts the correct level. However, it fails to predict the increase at $y/R\approx +0.5$, which is well reproduced by the DTU method and the highest peak, found at $y/R\approx 1.5$, is missing entirely. The Acona predictions have also placed the peaks at the right locations in Case A, but the levels are again much too low.

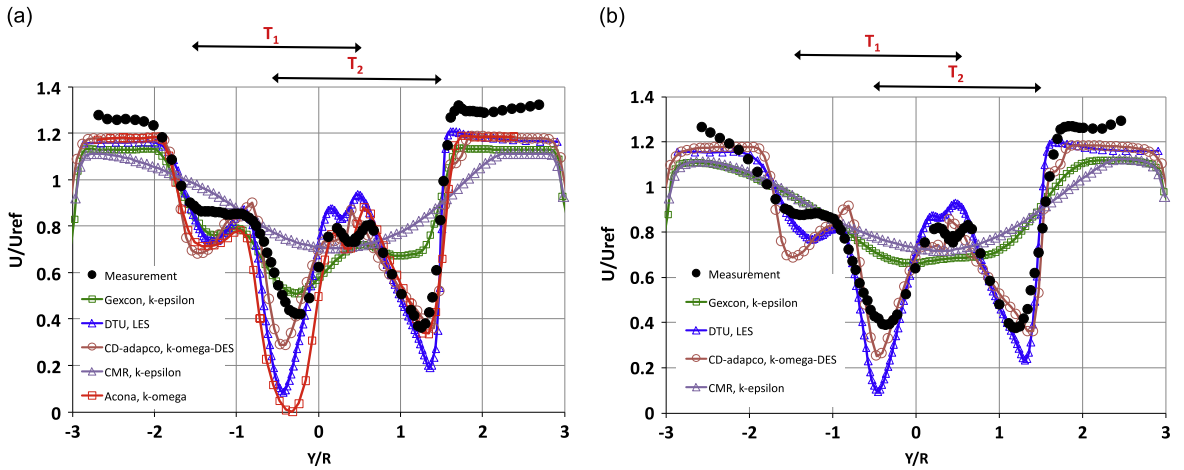

Fig. 18. Mean velocity profiles for $TSR_1=6$, $TSR_2=8.00$ at $X/D=1$. (a) Case A, (b) Case B. (For interpretation of the references to colour in this figure caption, the reader is referred to the web version of this paper.)

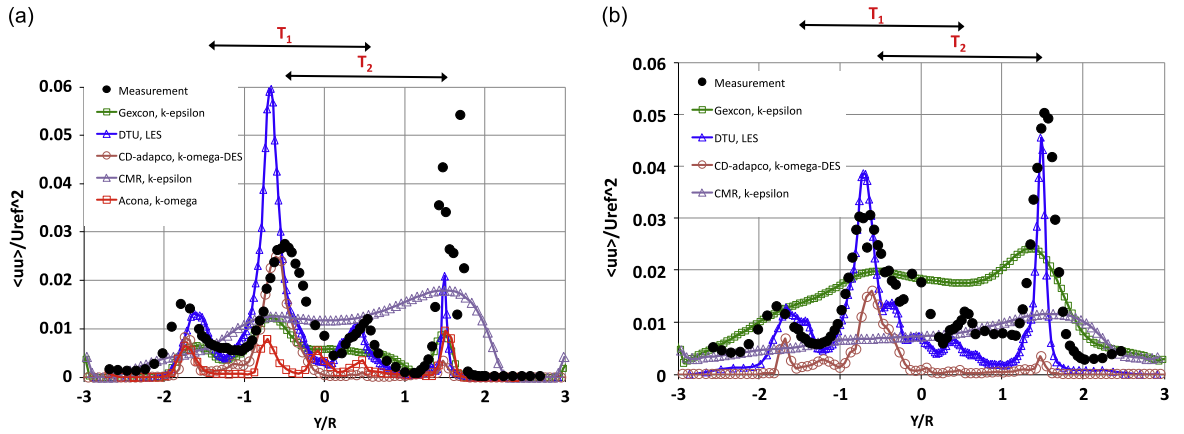

Fig. 19. Turbulent stress $\langle u_x^2 \rangle$ for $TSR_1=6$, $TSR_2=8.00$ at $X/D=1$. (a) Case A, (b) Case B. (For interpretation of the references to colour in this figure caption, the reader is referred to the web version of this paper.)

The method of GexCon is reasonably successful in Case A, but for Case B the profile is much too smooth. The CMR profiles once more lack most of the details in both cases.

Finally we will show the results at $X/D=3$ also for this case (Figs. 20 and 21). The figures show that there has been a remarkable change in all profiles between $X/D=1$ and 3, as most of the waviness seen at $X/D=1$ is lost by the time the flow reaches $X/D=3$. The mean velocity profiles generated by the methods of Acona and CD-adapco still show significant oscillations. While the Acona method predicted a very strong velocity defect on the left hand side of the T_2 wake at $X/D=1$, the strongest defect is at the right hand side at $X/D=3$. Since the kinetic energy predicted by this method has always been low, the reduction in the left side defect cannot be due to turbulent diffusion. Instead it suggests a very strong rotation in the wake, much more than what can be deduced from the measurements. This problem can be traced back to the very high C_P prediction for T_2 at $TSR_2=8.00$ (Fig. 7(a)). The strong diffusion in the GexCon predictions now makes it rather successful in reproducing Case A. For Case B the mean velocity profile of GexCon has too little velocity defect and the same applies to both cases for the CMR predictions.

The DTU turbulence predictions agree quite well with the measurements, especially for Case B, where the predicted profile matches the data almost perfectly. The oscillations in the profiles for both cases suggest that the sampling time of two complete passes through the computational domain probably was too short. The CD-adapco predictions are also in reasonable agreement with the measurements. The GexCon predictions have roughly the correct shape, with some indications of where high turbulence levels may be found, but the amplitudes are much too low in Case A. The predictions by CMR contain very little detail, while the Acona simulation of Case A seems to have retained too much waviness and therefore have underestimated the turbulent energy redistribution.

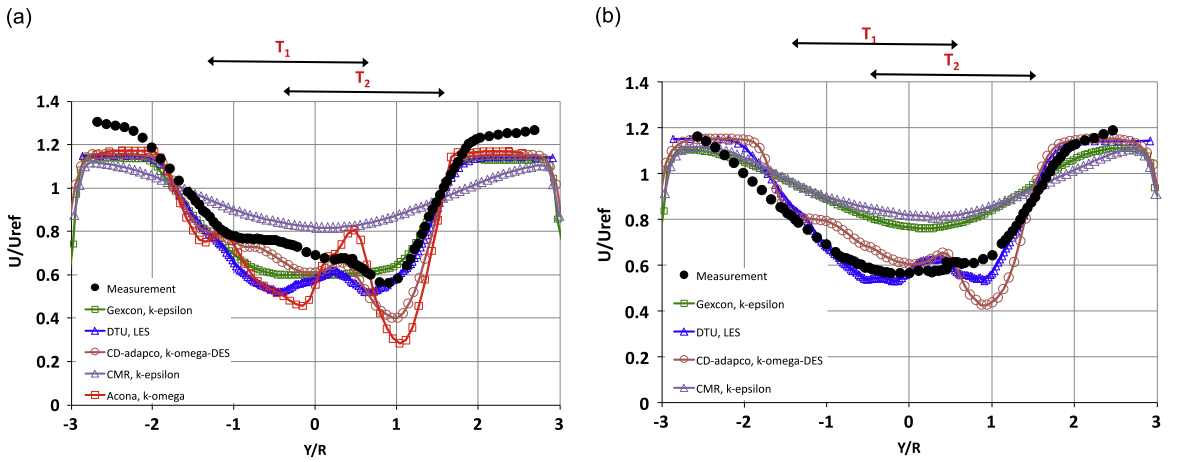

Fig. 20. Mean velocity profiles for $TSR_1=6$, $TSR_2=8.00$ at $X/D=3$. (a) Case A, (b) Case B. (For interpretation of the references to colour in this figure caption, the reader is referred to the web version of this paper.)

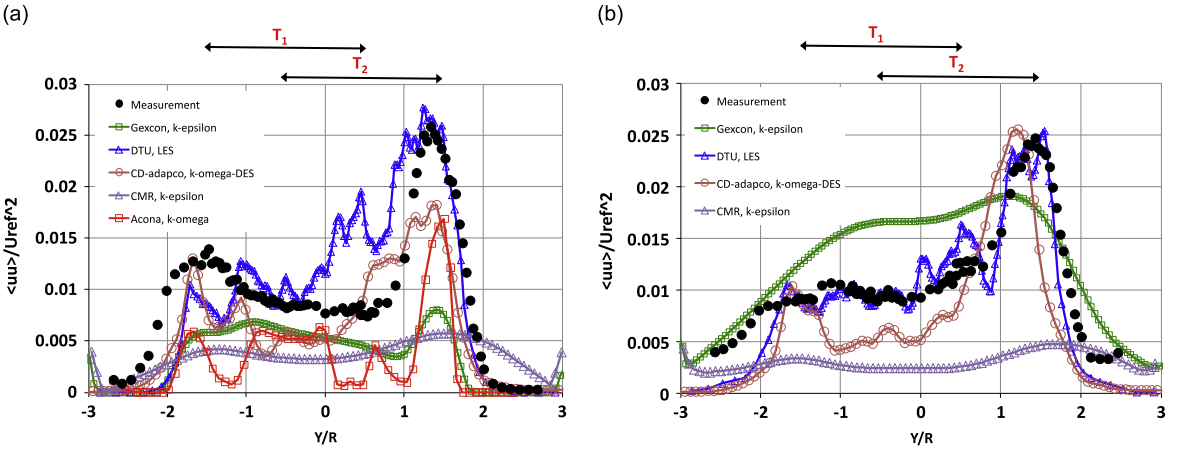

Fig. 21. Turbulent stress $\langle u_x^2 \rangle$ for $TSR_1=6$, $TSR_2=8.00$ at $X/D=3$. (a) Case A, (b) Case B. (For interpretation of the references to colour in this figure caption, the reader is referred to the web version of this paper.)

5. Some concluding remarks

This report describes the third wind turbine performance and wake development blind test arranged by Nowitech/Norcowe consisting of two turbines offset in the spanwise direction so that the wake from the first turbine only interacts with roughly half the area swept by the second rotor. To complicate the case even further we have added freestream turbulence to the flow.

The comparison between the model tests and predictions of the turbine performances and the wake development behind the second turbine have been presented in this report. Five research groups delivered simulation results. The methods ranged in complexity from standard commercial CFD methods to Large Eddy Simulations.

Even though the results from the two first blind tests are now well known, it was surprising that the performance data of the upstream turbine in a uniform, low turbulence flow still appear to be a challenge with results differing by about $\pm 10\%$ near the design condition. Obviously, if the performance of the upstream turbine is not correctly predicted, the results for the performance of the second turbine must be even more uncertain. And so the predictions of C_P for the downstream turbine showed a spread of about 50% of the measured values near the peak performance. Similar uncertainties were found for the predictions of the thrust coefficients.

For all cases investigated the upstream turbine was always operated at the same conditions, which was its best performance point (tip speed ratio of 6). This is the condition where the wake produced is the least complicated. But even when the second turbine is also operated at its best performance point (TSR ≈ 4.75 when scaled with the reference velocity at the test section inlet) the wake produced is very non-uniform with complicated interactions between the two wakes. Most methods captured this surprisingly well in the low turbulence case. However, it was a trend that the effects of turbulent diffusion were over-predicted by the methods using the k–ϵ turbulence model in the high turbulence cases, giving

a much smoother profile than in the measurements. Only the LES type methods did faithfully reproduce the data for both free stream conditions.

When the second turbine was operated off-design, either by reducing the tip speed until the flow over the blades was partly stalled (TSR = 3.5) or when the rotational speed was increased until the inner sections of the blades were feeding energy into the flow (TSR = 8.0), the flows became increasingly complicated. Again the LES method performed best, closely followed by a set of predictions using the k–ω SST DES model. Two groups used commercial CFD packages, while the other groups used software developed in-house. Two of these incorporated a k–ϵ turbulence model but produced very different results. This indicates that the choice of turbulence model is less critical than the implementation of grids and other choices which relies heavily on the judgement of the model operator. However, the predictions of the turbine performance data did show significant differences in the way the rotor was modelled, even when the same approaches were used; differences which automatically are carried over to the wake predictions.

The overall conclusion for this blind test was that the LES method produces the most reliable predictions and when the cases are set up properly, the results are very consistent when the boundary conditions are changed.

References

Adaramola, M., Krogstad, P.-Å., 2011. Experimental investigation of wake effects on wind turbine performance. Renewable Energy 36, 2078–2086.

Benedict, L., Gould, R., 1996. Towards better uncertainty estimates for turbulence statistics. Experiments in Fluids 22, 129–136.

Davidson, P., Krogstad, P.-Å., 2008. On the deficiency of even-order structure functions as inertial-range diagnostics. Journal of Fluid Mechanics 602, 287–302.

Drela, M., Xfoil 6.99 ⟨http://web.mit.edu/drela/Public/web/xfoil/⟩.

Hallanger, A., Sand, I.Ø., 2013. CFD Wake modelling with a BEM wind turbine sub-model. Modeling, Identification and Control 34, 19–33.

Khalil, M., Sælen, L., 2013. Near and far wake validation study for two turbines in line using two sub-grid turbine models. In: EWEA, Vienna, Austria, 4–7 February.

Krogstad, P.-Å., Adaramola, M., 2012. Performance and near wake measurements of a model horizontal axis wind turbine. Wind Energy 15, 743–756.

Krogstad, P.-Å., Eriksen, P., 2013. Blind test calculations of the performance and wake development for a model wind turbine. Renewable Energy 50, 325–333.

Krogstad, P.-Å., Lund, J., 2012. An experimental and numerical study of the performance of a model turbine. Wind Energy 15, 443–457.

Krogstad, P.-Å., Karlsen, J., Adaramola, M., 2010. Performance of a model wind turbine. In: 17 Australasian Fluid Mechanics Conference, Auckland, New Zealand, Paper 024, pp. 1–4.

Manger, E., 2011. Predictions for a model wind turbine: Power, trust and wake predictions using ansys fluent. Acona Flow Technology.

Mendonca, F., Baris, O., Capon, G., 2012. Simulation of radial compressor aeroacoustics using CFD. In: Proceedings of the ASME Turbo Expo 2012: Power for Land, Sea and Air, GT2012, pp. 1–10.

Pierella, F., Krogstad, P.-Å., Sætran, L., 2014. Blind Test 2 calculations for two in-line model wind turbines where the downstream turbine operates at three different rotational speeds. Renewable Energy 70, 62–77.

Schepers, J., Boorsma, K., Snel, H., 2010. IEA Task 29 MexNext: analysis of wind tunnel measurements from the EU project Mexico. In: Proceedings of The Science of Making Torque from Wind, pp. 169–178.

Schreck, S., 2002. Special issue: Analysis and modeling of the NREL Full-scale wind tunnel experiment. Wind Energy 5, 77–257.

Simms, D., Schreck, S., Hand, M., Fingersh, L., 2001. NREL Unsteady Aerodynamics Experiment in the NASA-Ames wind tunnel: A Comparison of Predictions to Measurements, National Renewable Energy Laboratory, Colorado, USA, NREL/TP-500-29494, pp. 1–44.

Snel, H., Schepers, J., Montgomerie, B., 2007. The Mexico (Model Experiments in Controlled Conditions): the data base and first results of data process and interpretation, Journal of Physics: Conference Series 75 (2007) 012014.

Troldborg, N., Sørensen, J., Mikkelsen, R., 2010. Numerical simulations of wake characteristics of a wind turbine in uniform inflow. Wind Energy 13, 86–99.